Empirical low-field mobility model for III–V compounds applicable in device simulation codes

M. Sotoodeh, A. H. Khalid, and A. A. Rezazadeh

Citation: Journal of Applied Physics **87**, 2890 (2000); doi: 10.1063/1.372274
View online: http://dx.doi.org/10.1063/1.372274
View Table of Contents: http://scitation.aip.org/content/aip/journal/jap/87/6?ver=pdfcov
Published by the AIP Publishing

Empirical low-field mobility model for III–V compounds applicable in device simulation codes

M. Sotoodeh, A. H. Khalid, and A. A. Rezazadeh[a)]
Department of Electronic Engineering, King's College London, Strand, London WC2R 2LS, United Kingdom

(Received 30 September 1999; accepted for publication 9 December 1999)

A Caughey–Thomas-like mobility model with temperature and composition dependent coefficients is used in this work to describe the dependence of electron and hole mobilities on temperature, doping concentration, and alloy composition. Appropriate parameter sets are given for a large number of III–V binary and ternary compounds, including: GaAs, InP, InAs, AlAs, GaP, $Al_{0.3}Ga_{0.7}As$, $In_{0.52}Al_{0.48}As$, $In_{0.53}Ga_{0.47}As$, and $In_{0.49}Ga_{0.51}P$. Additionally, physically justifiable interpolation schemes are suggested to find the mobilities of various ternary and quaternary compounds (such as $Al_xGa_{1-x}As$, $In_{1-x}Ga_xP$, $In_{1-x}Ga_xAs$, $In_{1-x}Al_xAs$, and $In_{1-x}Ga_xAs_yP_{1-y}$) in the entire range of composition. The models are compared with numerous measured Hall data in the literature and very good agreement is observed. The limitations of the present model are also discussed. The results of this work should be extremely useful in device simulation packages, which are currently lacking a reliable mobility model for the above materials. © *2000 American Institute of Physics.* [S0021-8979(00)03606-9]

I. INTRODUCTION

Electron and hole mobilities, μ_n and μ_p, are two of the most important parameters for characterizing the transport of charged carriers and formulating the current in semiconductor devices. A great deal of attention has been paid in the literature to these parameters and many authors have measured the carrier mobilities for various III–V compounds by Hall effect measurement technique. Plenty of effort has also been focused on theoretical formulation of minority and majority carrier mobilities in semiconductors (see, for instance, Refs. 1–3). In these analyses, a detailed physical formulation of various scattering mechanisms (such as ionized impurity scattering, acoustic phonon scattering, polar and nonpolar optical phonon scatterings, piezoelectric scattering, carrier–carrier scattering, and alloy scattering) has been made to accurately determine the variation of mobility with carrier concentration, temperature and, in some cases,[1] the compensation ratio. However, these approaches require accurate knowledge of some physical constants, like deformation potentials and alloy scattering potential, which are only available for widely studied semiconductors such as Si, GaAs, and InP. For ternary and quaternary compounds, the common approach is to use linear interpolations between the values for corresponding binaries.[4,5] But since the linear interpolation is proved to be not too realistic for some physical parameters (e.g., band gap and thermal conductivity), these parameters will finally be treated as adjustable fitting parameters. One common example of this case is alloy scattering potential which is a totally empirical parameter.[2,6] Additionally, the above techniques are sometimes too much mathematically involved and time consuming to be suitable for device simulation packages. Finally, some of the available scattering models are only applicable to limited ranges of carrier concentration and temperature. One good example of the latter is the Brooks–Herring model for ionized impurity scattering. In this model, which is used in almost all of the existing theoretical formulations of carrier mobility in the literature, the ionized impurity scattering limited mobility, μ_{II}, can be written as[7]

$$\mu_{II}=\frac{64\epsilon_s^2(2kT)^{3/2}}{q^3N_I}\sqrt{\frac{\pi}{m^*}}\cdot g_{BH}\left(\frac{24m^*\epsilon_s(kT)^2}{q^2\hbar^2N_I}\right), \tag{1}$$

where N_I is the ionized impurity concentration and all other parameters have their usual meanings. g_{BH} is the Brooks–Herring function of the form

$$g_{BH}(\gamma)=\left[\mathrm{Ln}(1+\gamma)-\frac{\gamma}{1+\gamma}\right]^{-1}. \tag{2}$$

It is straightforward to prove that in the limit of $\gamma\to 0$ (i.e., very small T or large N_I), the Brooks–Herring model generates some strange asymptotic behavior

$$\mu_{II}\propto\frac{N_I}{T^{5/2}(m^*)^{5/2}} \quad \text{for} \quad \gamma\to 0 \tag{3}$$

which means that at low temperatures (typically $T<50\,\mathrm{K}$) μ_{II} should increase either with further reduction of temperature or, more strangely, with increasing the doping concentration. Therefore, it is well known that the above model cannot be used for very small temperatures or high doping concentrations.

Having the above disadvantages of the accurate theoretical modeling in mind, in this work we decided to use an empirical model for carrier mobility. Models by Klaassen,[8] Caughey and Thomas,[9] Arora *et al.*,[10] and Noor Mohammad *et al.*[11] are examples of empirical mobility models. While other works were directed towards the mobility modeling

a)Electronic mail: ali.rezazadeh@kcl.ac.uk

primarily in silicon, the empirical model by Noor Mohammad *et al.*[11] was shown to be applicable to Si, Ge, GaAs, and InP. These latter authors started their model based on the Brooks–Herring formula for ionized impurity scattering limited mobility [Eq. (1)], but ended up with a mobility model which is always decreasing with temperature, opposite to the trend expected for ionized impurity scattering limited mobility. Additionally, their model suggests that if the low-field mobility of a particular material is known as a function of T and N_I, then the mobility of any other material will be obtained by simply scaling the same formula with a constant factor. The data presented in the following sections show that the latter assumption is far too simplistic.

In this work, a Caughey–Thomas-like mobility model with temperature dependent parameters is used. Parameters of this model are best fitted to the available Hall data for a wide range of carrier concentration and temperature using least-squares method. Additionally, these parameters are found for a large number of III–V binary, ternary, and quaternary compounds using both the available data and appropriate interpolation schemes. Available commercial device simulation packages such as MEDICI[12] and ATLAS[13] are currently lacking a realistic model for mobility of ternary and quaternary compounds. For instance, the mobility model in ATLAS[13] uses a linear interpolation to find the electron mobility in the quaternary material InGaAsP. This results in $\mu_n \sim 1750\ \mathrm{cm^2/V\,s}$ for $In_{0.1}Ga_{0.9}As_{0.1}P_{0.9}$, which seems unrealistic considering that this is an indirect band gap material. Additionally, no specific doping, temperature, or electric field dependence of mobility is given for ternary and quaternary materials such as InGaAsP in ATLAS. Therefore, the users of such simulation packages must provide their own functions or values for mobility of various regions with different doping concentrations and mole fractions, and at different temperatures. Hence, the results of the present work is expected to be of great importance for such simulation packages.

This article is organized as follows. The empirical mobility model will be first introduced in Sec. II, followed by its simplifying assumptions and range of validity in Sec. III. Then in Sec. IV parameters of the empirical model will be adjusted to give the best fit to available mobility data for some binary and ternary materials. Additionally, appropriate interpolation schemes are introduced to find those parameters in the entire range of composition for ternary and quaternary alloys. Finally, some conclusions are drawn in Sec. V.

II. LOW-FIELD MOBILITY MODEL

The low-field mobility model used in this work is expressed as

$$\mu_{\mathrm{LF}}(N,T)=\mu_{\min}+\frac{\mu_{\max}(300\ \mathrm{K})(300\ \mathrm{K}/T)^{\theta_1}-\mu_{\min}}{1+\left(\dfrac{N}{N_{\mathrm{ref}}(300\ \mathrm{K})(T/300\ \mathrm{K})^{\theta_2}}\right)^{\lambda}}, \tag{4}$$

where all the fitting parameters are non-negative. First we consider the physical sense of Eq. (4)

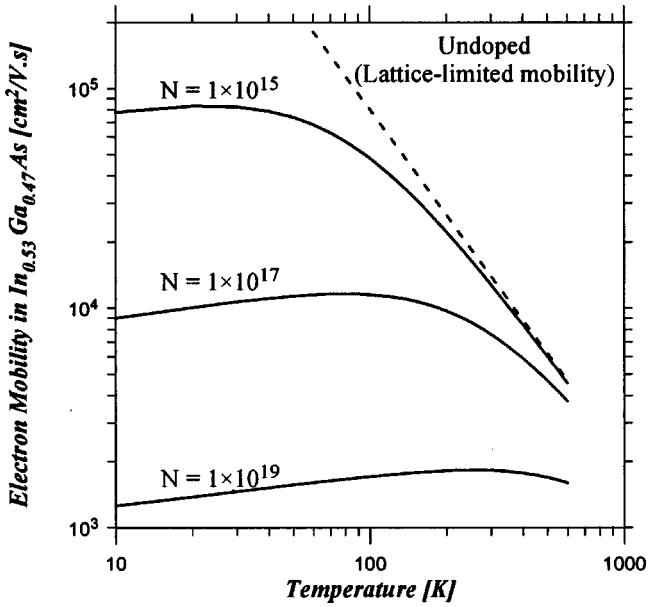

FIG. 1. Variation of low-field electron mobility in $In_{0.53}Ga_{0.47}As$ vs temperature with three different doping concentrations according to Eq. (4) and the parameters listed in Table I. The dashed line shows the lattice-limited mobility for an undoped sample, $\mu_{n,\max}(T)$.

1. At very low doping concentration, mobility saturates at $\mu_{\max}(T)$, the lattice-limited mobility, which itself reduces with increasing temperature ($\theta_1 > 0$).

2. At very high doping concentration, mobility saturates at $\mu_{\min}$, which is temperature independent. This is consistent with the fact that degenerate semiconductors show an almost temperature insensitive metal-like mobility. In particular, Lovejoy *et al.*[14] have shown that for *n*-type (*p*-type) GaAs samples doped to $\sim 4\times 10^{18}\ \mathrm{cm^{-3}}$ the majority electron (hole) mobility is almost constant at $\sim$2000 ($\sim$120) $\mathrm{cm^2/V\,s}$ for the temperature range $77\ \mathrm{K} < T < 300\ \mathrm{K}$.

3. $N_{\mathrm{ref}}(T)=N_{\mathrm{ref}}(300\ \mathrm{K})(T/300\ \mathrm{K})^{\theta_2}$ is the doping concentration at which mobility reduces to almost half of its maximum value at low doping. At higher temperatures lattice scattering mainly dominates, and therefore, the contribution of ionized impurity scattering is expected to start at larger doping concentrations. This is also consistent with the positive temperature power for $N_{\mathrm{ref}}(T)$ in Eq. (4) ($\theta_2 > 0$).

4. At high temperatures or low enough doping concentrations the temperature dependence of mobility is mainly determined by θ_1, which dictates a reduction of mobility with increasing T. However, as the temperature reduces, the term inside the bracket of the denominator in Eq. (4) starts to become important, even at relatively low doping concentration. Under this condition, the temperature power of $\mu_{\mathrm{LF}}(T)$ becomes $\sim(\lambda\theta_2-\theta_1)$. Consequently, mobility saturates at low T, and if $\lambda\theta_2 > \theta_1$ it finds a maximum, after which the mobility will be reduced with further reduction of temperature due to the dominance of ionized impurity scattering. This trend is exactly what the experimental Hall data for various semiconductors suggest. This property of the empirical function in Eq. (4), together with other properties addressed above, can be clearly seen in Fig. 1 in which the low-field mobility of $In_{0.53}Ga_{0.47}As$ is plotted as a function of temperature for three different doping concentrations.

5. The composition dependence of μ_{LF} is modeled by considering all the fitting parameters in Eq. (4) including μ_{min}, μ_{max} (300 K), N_{ref} (300 K), λ, θ_1, and θ_2 functions of composition x and y. Simplest possible interpolation schemes (linear, power, or quadratic interpolations) are used to find the ternary and quaternary parameters in the entire range of composition. These forms can be later modified to more complex functions as more data for intermediate ternary and quaternary materials become available. Of particular attention in this case must be the contribution of alloy scattering in ternary and quaternary compounds. Alloy scattering is shown to have a smoother variation with temperature than various mechanisms of lattice scattering, i.e., polar and nonpolar optical phonon and acoustic phonon scatterings (see, for instance, Ref. 6). Therefore, alloy scattering is expected to reduce both $\mu_{max}(300\,K)$ and θ_1 compared to the case where alloy scattering is ignored. As will be seen in the forthcoming parts, both $\mu_{max}(300\,K)$ and θ_1 will have a downward bowing (in the majority of materials) as the composition of ternary and quaternary materials varies.

III. LIMITATIONS

In the following, the limitations and the range of applicability of the above mobility model will be discussed:

1. The mobility data available in the literature are mainly measured using Hall effect technique and they give the majority carrier mobility versus majority carrier concentration. There are, however, instances where the minority carrier mobility would be of real concern, as in the base region of bipolar transistors. But, the techniques to measure the minority mobility are not straightforward, and consequently, their data are scarce and limited to only some well-studied semiconductors like Si, GaAs, and $Al_xGa_{1-x}As$. Therefore, in this work it has been assumed that the minority carrier mobility is the same as majority one. This assumption can cause large errors, since the variation of minority mobility with both doping concentration and temperature are shown to be significantly different from that of majority mobility. In particular, the minority electron mobility data for p-GaAs are summarized in Ref. 2. These data show that minority electron mobility is smaller than the majority one for $N_A < 10^{19}\,cm^{-3}$. But as the acceptor concentration increases above $10^{19}\,cm^{-3}$, the minority electron mobility starts to increase. The same trend has recently been observed for p-AlGaAs.[15] Theoretical calculation by Bennett[3] has also shown a good agreement to the above trend for GaAs and AlGaAs.

2. The measured ''Hall'' mobility (μ_H) can be significantly different from the ''drift'' mobility (μ_{drift}) when transport is due to carriers in two or more subbands.[2,16] The effective Hall factor determined as $r_H = \mu_H/\mu_{drift}$ can be as large as 4 for p-type III–V compounds in which hole transport occurs in the heavy and light hole subbands. Also for materials like $Al_xGa_{1-x}As$ and $In_{1-x}Ga_xP$, where a direct-to-indirect crossover may occur, the effective Hall factor for electrons increases near the crossover composition.[2] However, since the materials used in the majority of device applications are normally direct band gap materials sufficiently away from crossover composition, the effective Hall factor for electrons should not be of a prime concern. Additionally, it is shown by Wenzel *et al.*[16] that the hole effective Hall factor approaches unity as the doping concentration increases. This makes the assumption $\mu_H \approx \mu_{drift}$ valid in Npn heterojunction bipolar transistors (HBTs), for instance. However, this assumption should be reconsidered when compositions near direct-to-indirect crossover and/or lowly doped p-type materials are used.

3. Dopant compensation is ignored in this work. Considering the compensation makes the mobility model very complicated. Tables of mobility values for some III–V materials like GaAs,[17] and InP[18] are provided as a function of compensation ratio and total doping concentration at 77 and 300 K. But, unavailability of a similar set of data for other materials and also the disagreement of these tables with available experimental data in some ranges of doping concentration[19] prevents us from finding a general relation for compensation dependent mobilities. Consequently, uncompensated materials will be assumed throughout this work and $N_D + N_A$ will be used in place of N in Eq. (4).

4. Mobility is considered independent of the dopant species used. In fact, Anderson *et al.*[19] have measured the electron Hall mobilities for a large number of InP samples doped with Si, S, Sn, Se, and Ge to the levels between 10^{15} and $10^{19}\,cm^{-3}$. Their results showed nearly identical electrical behavior for all n-type dopants. On the other hand, the study of hole mobility in p-GaAs has revealed that C-doped GaAs has almost 20%–30% higher mobility than Zn- or Be-doped GaAs with the same amount of hole concentration (Ref. 20). These strikingly different results to those of InP may be due to the different compensation ratio in C-doped GaAs compared to other p-type dopants.

5. It is also assumed that mobility is independent of the growth method. In the next section it will be shown that metal organic chemical vapor deposition (MOCVD) grown n-$In_{0.49}Ga_{0.51}P$ generally has higher electron mobility than molecular beam epitaxy (MBE), gas source MBE (GSMBE), and liquid phase epitaxy (LPE) samples. This is contradicting the present assumption, but again might be due to different levels of compensation for various growth methods.

6. Effects like carrier–carrier scattering and surface scattering [very important for field-effect transistors (FET)] are not considered.

7. The model is valid for relatively thick epitaxially grown materials. Effects like mobility enhancement due to modulation doping in modulation doped field effect transistor (MODFETs) which form two-dimensional electron gas (2DEG) are not considered.

8. Although Eq. (4) generates a reasonable ''trend'' for variation of mobility at low temperatures (i.e., saturation of mobility and sometimes reduction of it with further decreasing temperature), it is not particularly attempted to fit this equation to the available experimental data for $T < 100-150\,K$. This attempt may, for example, need a temperature dependent λ in Eq. (4). Therefore, this mobility model should be used with caution at temperatures lower than 100–150 K.

TABLE I. Fitting parameters for the low-field mobility model in Eq. (4).

Material	Electron or hole	μ_{max} (300 K) ($cm^2/V\,s$)	μ_{min} ($cm^2/V\,s$)	N_{ref} (300 K) cm^{-3}	λ	θ_1	θ_2
AlAs	electron	400	10	5.46×10^{17}	1.00	2.1	3.0
	hole	200	10	3.84×10^{17}	0.488	2.24	3.0
GaAs	electron	9400	500	6.0×10^{16}	0.394	2.1	3.0
	hole	491.5	20	1.48×10^{17}	0.38	2.2	3.0
InAs	electron	34 000	1000	1.1×10^{18}	0.32	1.57	3.0
	hole	530	20	1.1×10^{17}	0.46	2.3	3.0
InP	electron	5200	400	3.0×10^{17}	0.47	2.0	3.25
	hole	170	10	4.87×10^{17}	0.62	2.0	3.0
GaP	electron	152	10	4.4×10^{18}	0.80	1.60	0.71
	hole	147	10	1.0×10^{18}	0.85	1.98	0.0
$Al_{0.3}Ga_{0.7}As$	hole	240	5	1.0×10^{17}	0.324	⋯	⋯
$In_{0.52}Al_{0.48}As$	electron	4800	800	3.0×10^{16}	1.10	⋯	⋯
$In_{0.53}Ga_{0.47}As$	electron	14 000	300	1.3×10^{17}	0.48	1.59	3.68
	hole	320	10	4.9×10^{17}	0.403	1.59	⋯
$In_{0.49}Ga_{0.51}P$	electron	4300	400	2.0×10^{16}	0.70	1.66	⋯
	hole	150	15	1.5×10^{17}	0.80	2.0	⋯

The above assumptions may sometimes seem very harsh and the reader may conclude that the final product will be only of a very limited application. However, it should be considered that many of the above assumptions may be completely satisfied for a particular device, and those which are not, may act in opposing directions. Indeed, as is shown in the next subsection, Eq. (4) creates very good fits to the available data for a wide range of III–V materials, temperature, and doping concentration.

IV. FITTING PARAMETERS FOR THE LOW-FIELD MOBILITY

Table I summarizes the fitting parameters of Eq. (4) for various binary and ternary compounds. These parameters together with their variation with composition for ternary and quaternary compounds will be discussed individually in the forthcoming subsections.

A. GaAs

Electron and hole Hall mobilities of GaAs have been measured by many groups and a large number of data are available in the literature. References 2, 20, and 21, in particular, include excellent compilations of the data and useful references for further studies. Additionally, measured data by various authors show a relatively good consistency in the carrier concentration range 1×10^{13}–$2\times10^{19}\,cm^{-3}$ for *n*-type and 1×10^{14}–$2\times10^{21}\,cm^{-3}$ for *p*-type GaAs. This allows us to find an accurate set of parameters for low-field mobilities in GaAs. Figures 2 and 3 show some of the available room temperature data for *n*- and *p*-type GaAs, respectively, together with the empirical fits made by the parameter sets given in Table I. As mentioned previously in Sec. III, the hole mobility of GaAs doped with C is almost 20%–30% higher than that of Zn- or Be-doped GaAs (Ref. 20). The parameters obtained in this work best fit the data for C-doped GaAs at concentrations above $10^{18}\,cm^{-3}$.

The parameters θ_{n1} and θ_{p1} are found using the temperature dependence of mobility for relatively pure materials. It is generally observed that μ_n(GaAs) drops sharply with increasing temperature ($\theta_{n1}=2.59$) in the temperature range $70\,K<T<300\,K$, but the fall-off becomes slower for $300\,K<T<900\,K$ (Ref. 6). Values of θ_{n1} in the range 2.0–2.3 can be fitted to the data available in (Refs. 20,25) for the medium range of temperature. $\theta_{n1}=2.1$ used in this work seems to produce very good fit to the available data for $100\,K\leqslant T\leqslant400\,K$, and even above 400 K the error would not be large. θ_{p1} in the range of 2.0–2.5 can be best fitted to the data in (Refs. 2,6,20,25), and is also mentioned by other authors.[26,27] $\theta_{p1}=2.2$ is chosen in this work with the valid temperature range $100\,K\leqslant T\leqslant400\,K$.

In order to find θ_2, one needs to have the concentration dependence of mobility at temperatures other than 300 K. Unfortunately, the only other temperature for which reliable concentration dependent data are available for majority of

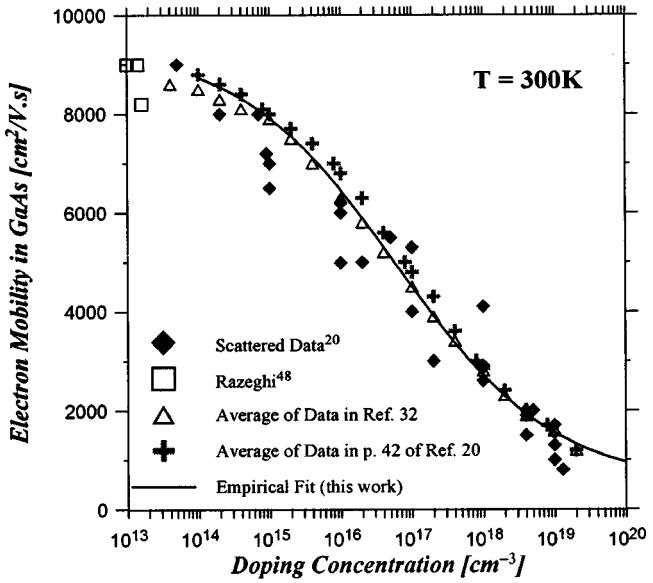

FIG. 2. GaAs electron mobility data vs doping concentration at room temperature, together with the empirical fitting obtained in this work. Due to the large number of data in the graphs of Ref. 20 and Ref. 32, only some points representing the averages of these data are shown.

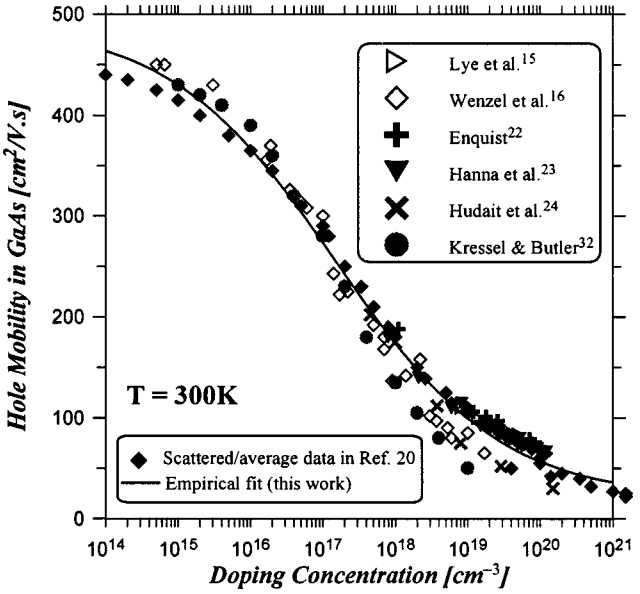

FIG. 3. GaAs hole mobility data vs doping concentration at room temperature, together with the empirical fit obtained in this work. The experimental data are taken from numerous sources (see Refs. 15, 16, 20, 22–24, and 32).

III–V materials is 77 K, that is not lying within the range of validity of the mobility models in this work. However, assuming that the temperature dependence of $N_{\rm ref}$ remains the same outside the range of validity of our mobility model, one can use $N_{\rm ref}(77\,{\rm K})$ to find an estimate of θ_2. Using the data compiled in Ref. 21 one finds $N_{n,{\rm ref}}({\rm GaAs},77\,{\rm K})\approx 1.0\times 10^{15}\,{\rm cm}^{-3}$, which results in $\theta_{n2}\approx 3.0$. This value is similar to the one obtained for silicon,[28] and will be used as default throughout this work wherever reliable data is not available. For $\theta_{p2}({\rm GaAs})$ this default value is used.

B. AlAs and $Al_xGa_{1-x}As$

The parameters for the electron mobility in AlAs are chosen to give the best least-square fits to the data in Ref. 2. Due to the lack of experimental data, it is assumed that θ_{n1} and θ_{n2} in AlAs are the same as those in GaAs. As to the electron mobility in $Al_xGa_{1-x}As$ as a function of Al mole fraction, the situation is a bit more complicated. Since the electron effective mass of AlGaAs increases almost abruptly as the Al mole fraction, x, approaches the direct-to-indirect crossover point ($x\sim 0.4$), a sudden drop of electron mobility near the same composition level is expected theoretically (and observed experimentally, as the following results suggest). This form of mobility variation can be taken into account by a similar variation in $\mu_{n,\max}(300\,{\rm K})$ and $\mu_{n,\min}$. The formulation of the latter two parameters in this work follows that suggested by Sutherland and Hauser.[29] When multivalley conduction takes place, an effective mobility can be defined as

$$\mu_M(x)=\frac{n_\Gamma(x)\mu_D(x)+[n_X(x)+n_L(x)]\mu_I(x)}{n}, \tag{5}$$

where $\mu_D(x)$ and $\mu_I(x)$ represent the effective electron mobility in the direct and indirect conduction valleys, respectively, μ_M stands for either $\mu_{n,\max}(300\,{\rm K})$ or $\mu_{n,\min}$ in $Al_xGa_{1-x}As$, n_ν ($\nu=\Gamma$, X, or L) is the concentration of electrons in the corresponding conduction band minima,[29] and n is the total electron concentration. For the formulation of the direct band mobility, it is assumed that mobility of AlGaAs is dominated by polar optical phonon scattering, and therefore[29]

$$\mu_D(x)\propto\frac{1}{(m_{n\Gamma}(x))^{3/2}[\varepsilon_\infty^{-1}(x)-\varepsilon_s^{-1}(x)]}, \tag{6}$$

where $m_{n\Gamma}$ is the effective mass of electrons in the Γ-conduction band, and $\varepsilon_\infty,\varepsilon_s$ are the optical and static dielectric constants, respectively. Hence, using the mobility of (direct bandgap) GaAs as one end of this composition range, one can write

$$\mu_D(Al_xGa_{1-x}As)=\mu_M({\rm GaAs})\left[\frac{m_{n\Gamma}({\rm GaAs})}{m_{n\Gamma}(x)}\right]^{3/2}\times\frac{\varepsilon_\infty^{-1}({\rm GaAs})-\varepsilon_s^{-1}({\rm GaAs})}{\varepsilon_\infty^{-1}(x)-\varepsilon_s^{-1}(x)}. \tag{7}$$

Values of the effective masses and dielectric constants for binary compounds together with the appropriate interpolation schemes to find these parameters in ternaries are summarized in the Appendix. A similar formulation can be used to find $\mu_I(Al_xGa_{1-x}As)$, this time replacing the parameters of GaAs with those of (indirect band gap) AlAs. But since the electron mobility at the X valley for both AlAs (see Table I) and GaAs (see below) are known, a linear interpolation between the two binary ends would be a reasonable choice. It is well known that at pressures above ~40 kbar the X valley of GaAs lies below the Γ valley, and therefore, the electron mobility measured at pressures extending 40 kbar would represent the X-valley mobility in this material. A plot of GaAs X-valley Hall mobility at 50 kbar and room temperature is shown in Ref. 2 as a function of impurity concentration. It can be seen from this figure that the variation of $\mu_{nX}({\rm GaAs})$ with doping is very similar to that of $\mu_n({\rm AlAs})$. Therefore, a linear interpolation between the values of the two binaries will result in

$$\mu_I(Al_xGa_{1-x}As)=\mu_M({\rm AlAs}). \tag{8}$$

As mentioned previously, the above formulation can be used to find both $\mu_{n,\max}(300\,{\rm K})$ and $\mu_{n,\min}$. The two parameters λ_n and θ_{n2} are linearly interpolated between the corresponding values of the binaries. Since the range of variation for $N_{n,{\rm ref}}$ is usually much wider than other parameters, a power interpolation of the following form may be used

$$N_{n,{\rm ref}}(Al_xGa_{1-x}As)=[N_{n,{\rm ref}}({\rm GaAs})]^{(1-x)}\times[N_{n,{\rm ref}}({\rm AlAs})]^x. \tag{9}$$

To take the downward bowing of $\theta_{n1}(x)$ due to alloy scattering into account, an interpolation formula of the form

$$\theta_{n1}(Al_xGa_{1-x}As)=\frac{(1-x)\,\theta_{n1}({\rm GaAs})+x\,\theta_{n1}({\rm AlAs})}{1+mx(1-x)} \tag{10}$$

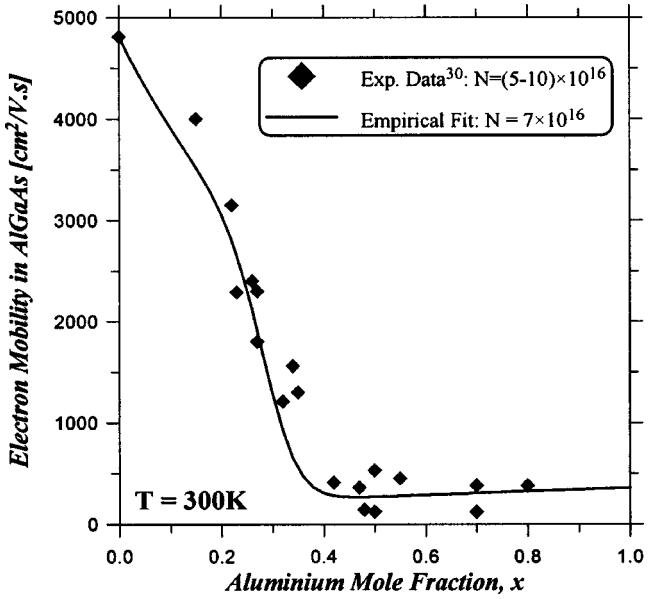

FIG. 4. Calculated room temperature electron mobility of $Al_xGa_{1-x}As$ with $N=7\times10^{16}\,cm^{-3}$ as a function of Al mole fraction, x. Also shown are the experimental Hall data (Ref. 30) for the doping range $(5-10)\times10^{16}\,cm^{-3}$.

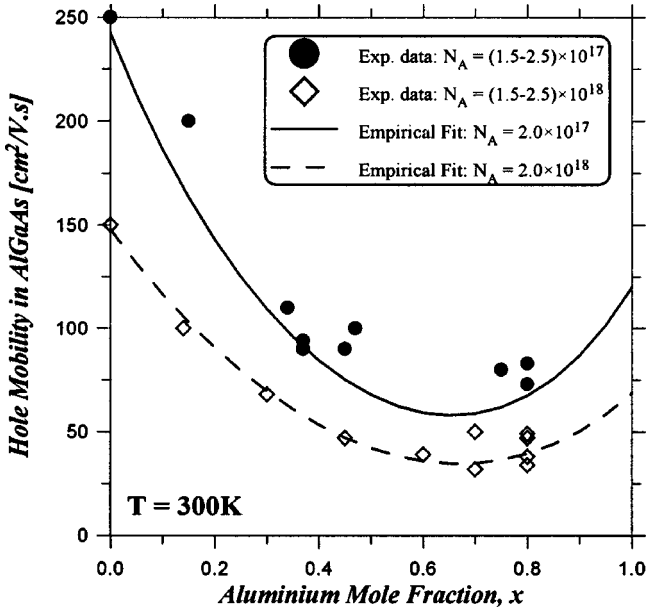

FIG. 5. The experimental hole mobility data (see Refs. 30 and 31) for AlGaAs for the doping ranges $(1.5-2.5)\times10^{17}$ and $(1.5-2.5)\times10^{18}\,cm^{-3}$, together with the calculated mobilities in this work for $N_A=2\times10^{17}$ and $2\times10^{18}\,cm^{-3}$.

can be suggested. It is found that $m=1$ gives a reasonable agreement to the temperature dependent electron mobility data for $x=0.32$, 0.36 in Ref. 2.

As a confirmation of the above mobility formulation, the room temperature electron mobility of $Al_xGa_{1-x}As$ with $7\times10^{16}\,cm^{-3}$ doping concentration is plotted in the entire composition range in Fig. 4. Also shown in this figure are the measured Hall data in the literature (summarized in Ref. 30) for the doping concentration range $(5\times10^{16}-1\times10^{17})\,cm^{-3}$. An excellent agreement has been found for the entire range of composition.

The parameters of $\mu_p(Al_{0.3}Ga_{0.7}As)$ in Table I are obtained from fitting to the room temperature mobility data in Ref. 2. To the best of authors' knowledge no Hall mobility data is available for *p*-type AlAs in the literature. However, due to the similarities between the band structure of AlAs and GaP, it is expected that AlAs has a similar hole mobility to GaP (to be discussed later in this section). The room temperature hole mobility parameters of AlAs in this work are chosen such that quadratic interpolation between the parameters of GaAs, $Al_{0.3}Ga_{0.7}As$, and AlAs results in good agreement to the available data for $0\leqslant x\leqslant0.8$ (see Fig. 5). Figure 5 shows the available experimental hole mobilities of AlGaAs$(0\leqslant x\leqslant0.8)$ for the doping ranges $(1.5-2.5)\times10^{17}$ and $(1.5-2.5)\times10^{18}\,cm^{-3}$ (Refs. 30 and 31), together with the calculated values in this work for $N_A=2\times10^{17}$ and $2\times10^{18}\,cm^{-3}$, respectively. The agreement is very good. As mentioned earlier, the room temperature parameters of μ_p(AlGaAs), i.e., $\mu_{p,\max}(300\,K)$, $\mu_{p,\min}$, λ_p, and $\log_{10}(N_{p,\mathrm{ref}})$, are obtained by quadratic interpolations between the corresponding parameters of GaAs, AlAs, and $Al_{0.3}Ga_{0.7}As$. $\theta_{p1}(\mathrm{AlAs})=2.24$ can be obtained from the calculated temperature dependent figure in (Ref. 2) for $100\,K<T<400\,K$, and θ_{p1}(AlGaAs) can be found similar to θ_{n1}(AlGaAs) [Eq. (10)] using $m=1$. Due to the lack of experimental data, θ_{p2}(AlGaAs) is assumed to be equal to θ_{p2}(GaAs).

C. InP

Electron Hall mobility of InP has been measured and compiled by various authors.[19,32–36] Anderson *et al.*[19] have extensively studied the electron mobility in numerous InP samples doped with Si, S, Se, Ge, or Sn, in a wide range of doping concentration $(10^{15}-5\times10^{19})\,cm^{-3}$ at $T=77$ and 300 K. Their data for various dopants show very good consistency in the entire range of doping concentration, and therefore, it is the tabulated average of these data which forms the basis for empirical fitting in this work. The average of the 300 K data in Ref. 19 together with other data in the literature and the empirical fit obtained in this work are shown in Fig. 6. Additionally, from fitting to the 77 K data in Ref. 19 one can obtain $N_{n,\mathrm{ref}}(\mathrm{InP},77\,K)=3.6\times10^{15}\,cm^{-3}$, which together with the room temperature value of this parameter results in $\theta_{n2}(\mathrm{InP})=3.25$. Also $\theta_{n1}(\mathrm{InP})=2.0(100\,K<T<300\,K)$ is used in this work as suggested in Refs. 6 and 25.

The hole mobility in InP has also received considerable attention in the literature. Figure 7 summarizes the reported data.[16,25,33,37–39] Again the empirical fit in this work shows a very good agreement to the above data. Values of θ_{p1}(InP) in the range of 1.9–2.2 can be found from the data in Refs. 6, 25, 33, and $\theta_{p1}(\mathrm{InP})=2.0$ is adopted in the present work. Also $\theta_{p2}(\mathrm{InP})=3.0$ (default value) is assumed.

D. GaP

The electron and hole mobilities in GaP are measured as a function of both temperature and carrier concentration by

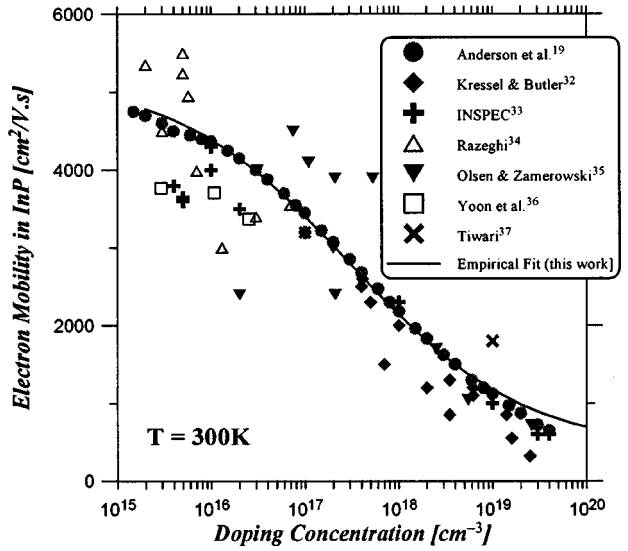

FIG. 6. Room temperature electron mobility data for InP from various sources, together with the empirical fit obtained in this work.

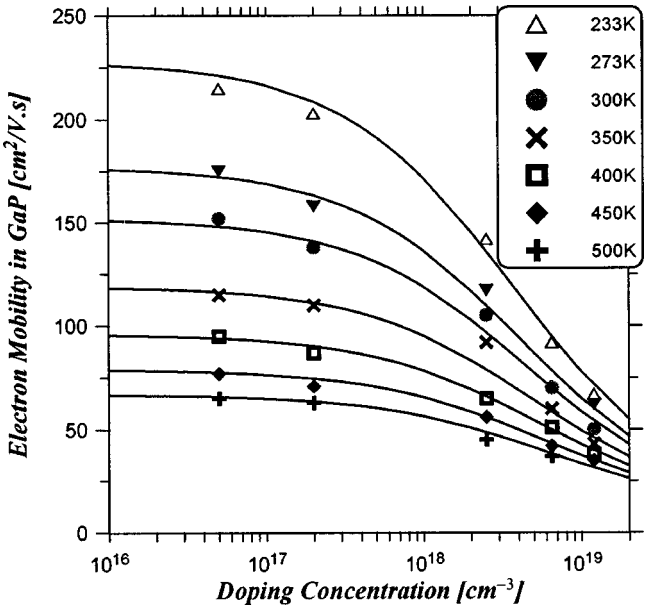

FIG. 8. The measured Hall electron mobility (symbols) (see Ref. 40) and the empirical fit obtained in this work (solid lines) for GaP as a function of both temperature and doping concentration.

Kao and Eknoyan,[40] and these data are used in this work to obtain all the fitting parameters in Eq. (4) for GaP. The empirical fit explained by Eq. (4) together with the parameter sets given in Table I agree very well to the measured μ_n(GaP) and μ_p(GaP) in a wide range of temperature and doping concentration, as shown in Figs. 8 and 9. Also the room temperature variation of μ_p(GaP) with doping concentration in Fig. 9 agrees very well with the data from other resources[16,32] (not shown in this figure).

E. $In_{1-x}Ga_xP$

The room temperature electron mobility of $In_{0.49}Ga_{0.51}P$ is measured by various groups[41–58] and they are summarized in Fig. 10. As can be seen in this figure, the MOCVD grown samples clearly have larger mobilities than their MBE, GSMBE, metal organic MBE (MOMBE), and LPE counterparts. The parameters given in Table I are best suitable for MOCVD grown samples. It is also worth mentioning that some undoped MOCVD samples with very large electron mobilities ($>$6000 cm^2/V s) are reported by Razeghi[48] which are not considered for the curve fitting in this work. From the temperature dependent data in Ref. 45, $\theta_{n1}(In_{0.49}Ga_{0.51}P) = 1.66$ can be obtained.

$\mu_p(In_{0.49}Ga_{0.51}P)$ has also been reported by various authors,[44–50,59,60] and in this case samples with different growth techniques do not show any striking difference in

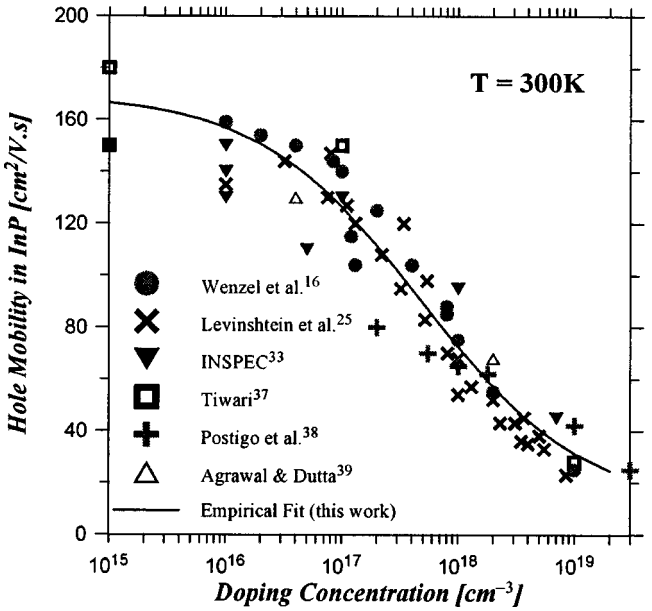

FIG. 7. Room temperature hole mobility data for InP from various sources, together with the empirical fit obtained in this work.

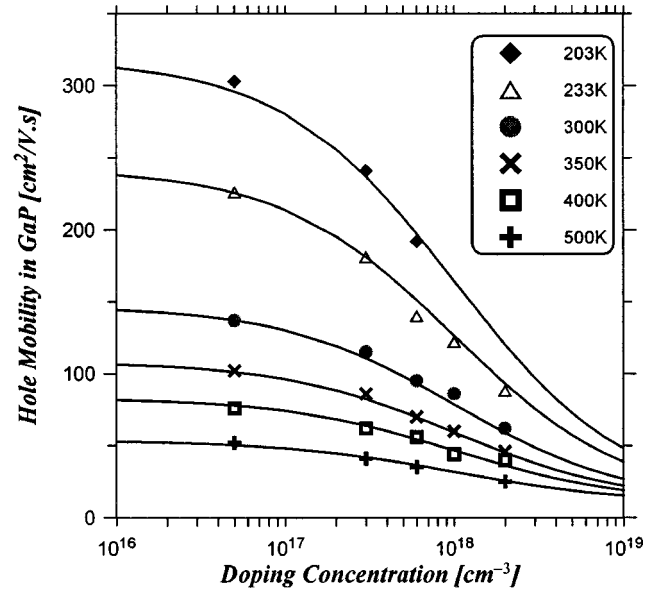

FIG. 9. The measured Hall hole mobility (symbols) (see Ref. 40) and the empirical fit obtained in this work (solid lines) for GaP as a function of both temperature and doping concentration.

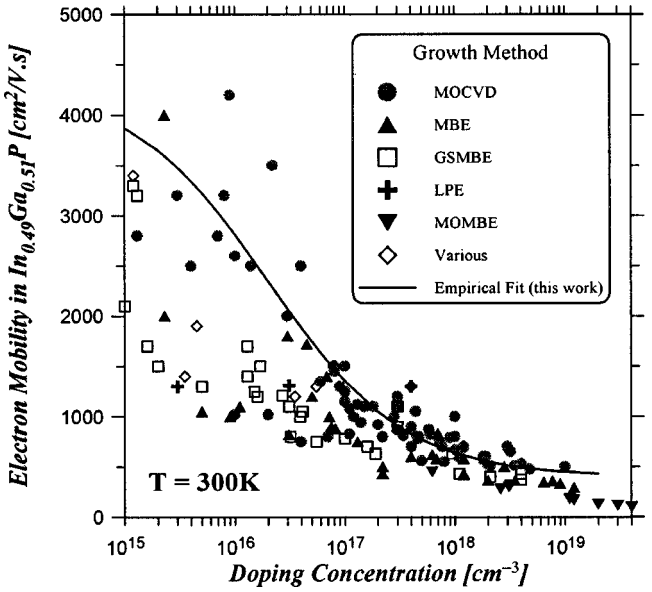

FIG. 10. The room temperature data for MOCVD-, MBE-, GSMBE-, MOMBE-, and LPE-grown $In_{0.49}Ga_{0.51}P$ reported by various authors (see Refs. 41–58). The calculated curve in this work (solid line) passes through the average of the reported MOCVD data.

their hole mobility. Room temperature parameters listed in Table I best fit to the above data. From the hole mobility data for $In_{0.49}Ga_{0.51}P$ with $5.14\times10^{17}\,cm^{-3}$ hole concentration,[45] a temperature dependence proportional to $(300\,K/T)^{1.76}$ could be obtained for $150\,K<T<300\,K$. But considering the fact that lower doped samples show sharper variation of mobility with temperature, a value of $\theta_{p1}(In_{0.49}Ga_{0.51}P)=2.0$ seems appropriate for relatively low doped materials.

As to the parameters of $In_{1-x}Ga_xP$, a linear interpolation between the values of the binaries will be used for finding θ_{n2} and θ_{p2}. The parameters θ_{n1}, θ_{p1}, λ_n, λ_p, $\mathrm{Log}_{10}[N_{n,\mathrm{ref}}(300\,K)]$, $\mathrm{Log}_{10}[N_{p,\mathrm{ref}}(300\,K)]$, $\mu_{p,\min}$, and $\mu_{p,\max}(300\,K)$ are found using a quadratic interpolation between the corresponding values for InP, $In_{0.49}Ga_{0.51}P$, and GaP. $\mu_{n,\max}(In_{1-x}Ga_xP,300\,K)$ is calculated in a way similar to $Al_xGa_{1-x}As$, i.e., Eq. (5). However, in this case $\mu_D(x)$ is obtained by a linear interpolation between the maximum mobilities in the direct band gap materials InP and $In_{0.49}Ga_{0.51}P$

$$\mu_D(x)=\left(1-\frac{x}{0.51}\right)\mu_{n,\max}(\mathrm{InP},300\,K)+\left(\frac{x}{0.51}\right)\mu_{n,\max}(In_{0.49}Ga_{0.51}P,300\,K) \tag{11}$$

and a theoretical mobility variation is used for the indirect valley mobility, μ_I, based on the assumption that electron mobility in InGaP is dominated by polar optical phonon scattering

$$\mu_I(x)=\mu_{n,\max}(\mathrm{GaP},300\,K)\times\left[\frac{m_{n,\mathrm{indir}}(\mathrm{GaP})}{m_{n,\mathrm{indir}}(x)}\right]^{3/2}\frac{\varepsilon_\infty^{-1}(\mathrm{GaP})-\varepsilon_s^{-1}(\mathrm{GaP})}{\varepsilon_\infty^{-1}(x)-\varepsilon_s^{-1}(x)}, \tag{12}$$

where $m_{n,\mathrm{indir}}(\mathrm{GaP})\approx m_{nX}(\mathrm{GaP})$ and $m_{n,\mathrm{indir}}(x)$ is an appropriately defined effective mass[61] which takes into account the relative position of the indirect valleys X and L in $In_{1-x}Ga_xP$ as a function of x. A similar approach to the above is used to find $\mu_{n,\min}(In_{1-x}Ga_xP)$.

F. InAs

The room temperature electron and hole mobility parameters of InAs in Table I are chosen to give reasonable agreement to the data mainly in Ref. 25 and few others reported elsewhere.[32,37,62] The large value of $N_{n,\mathrm{ref}}=1.1\times10^{18}\,cm^{-3}$ and the small value of $\lambda_n=0.32$ are consistent with the large number of data shown in Ref. 25 which suggest that for $N_D<4\times10^{17}\,cm^{-3}$, $\mu_n(\mathrm{InAs})$ does not change significantly with doping. $\theta_{n1}(\mathrm{InAs})=1.57$ can reproduce the temperature dependent electron mobility data in Ref. 25 reasonably well in the temperature range $150\,K<T<900\,K$. Also $\theta_{p1}(\mathrm{InAs})=2.3$ is reported in (Ref. 6) for $T>250\,K$. Finally, due to the lack of data, the default value of 3.0 is allocated to both θ_{n2} and θ_{p2} in InAs.

G. $In_{1-x}Ga_xAs$

First, the fitting parameters of the composition lattice matched to InP are considered. The electron mobility parameters in $In_{0.53}Ga_{0.47}As$ are fitted to the average of the low doping data in (Refs. 33,34,63 and 64) and mainly to the high doping data in Ref. 65. $\theta_{n1}(In_{0.53}Ga_{0.47}As)=1.59(100\,K<T<300\,K)$ can be fitted to the temperature dependent mobility data in Ref. 6. A value of $N_{n,\mathrm{ref}}(In_{0.53}Ga_{0.47}As,77\,K)=8.7\times10^{14}\,cm^{-3}$ can be obtained from fitting to the 77 K Hall data mainly in Refs. 34 and 63, which results in $\theta_{n2}(In_{0.53}Ga_{0.47}As)=3.68$. The room temperature hole mobility parameters of $In_{0.53}Ga_{0.47}As$ are fitted to the rather limited data in Refs. 63 and 64. $\theta_{p1}=\theta_{n1}$ is also assumed for $In_{0.53}Ga_{0.47}As$.

All the electron and hole mobility parameters of $In_{1-x}Ga_xAs$ are quadratically interpolated between the corresponding parameters of GaAs, InAs, and $In_{0.53}Ga_{0.47}As$, except θ_{p2}, $N_{n,\mathrm{ref}}(300\,K)$, and $N_{p,\mathrm{ref}}(300\,K)$. $\theta_{p2}(In_{1-x}Ga_xAs)=\theta_{p2}(\mathrm{GaAs})$ is assumed, and the logarithms of the other two parameters are quadratically interpolated between the known values for the three compositions. It is worth noting that the values of $\mu_{\max}(300\,K)$ and θ_1 (both for electrons and holes) given in Table I automatically produce downward bowing for these parameters in the ternary compound $In_{1-x}Ga_xAs$, taking the effects of alloy scattering into account.

H. $In_{1-x}Al_xAs$

Recently Goto *et al.*[66] presented a large number of data for electron mobility of $In_{0.52}Al_{0.48}As$ in samples with Hall electron concentrations in the range $(5\times10^{16}-6\times10^{18})\,cm^{-3}$. Although these data show some discrepancy due to the variation of growth parameters, they together with few other experimental and theoretical data available in Ref. 63 form the basis for the selection of room temperature parameters of $\mu_n(In_{0.52}Al_{0.48}As)$ in Table I.

As to the parameters for $\mu_n(In_{1-x}Al_xAs)$, the maximum mobility is found using a method similar to that used for $In_{1-x}Ga_xP$. However, due to the large difference in the electron mobilities for InAs and $In_{0.52}Al_{0.48}As$, a linear interpo-

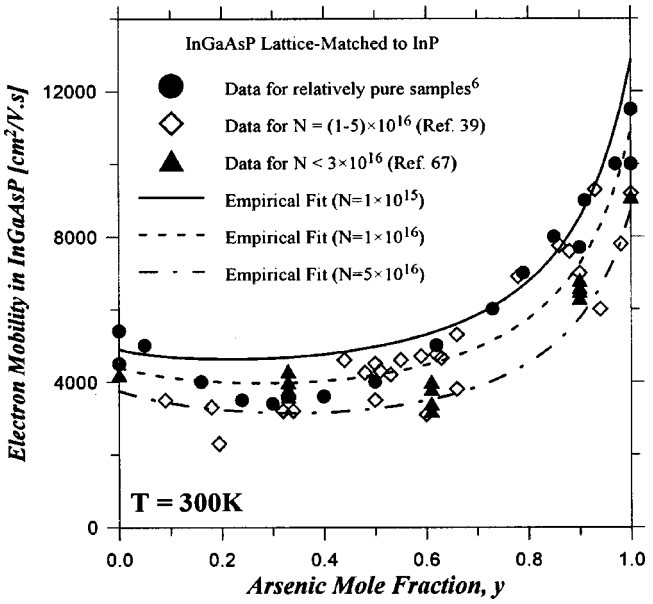

FIG. 11. Electron mobility data of InGaAsP lattice matched to InP vs arsenic mole fraction for the doping range $(1-5)\times10^{16}\,\mathrm{cm}^{-3}$ (open diamonds) (see Ref. 39), for $N<3\times10^{16}\,\mathrm{cm}^{-3}$ (solid triangles) (see Ref. 68), and for relatively pure samples (solid circles) (see Ref. 6). The experimental Hall data are compared with the empirical curves obtained in this work (lines).

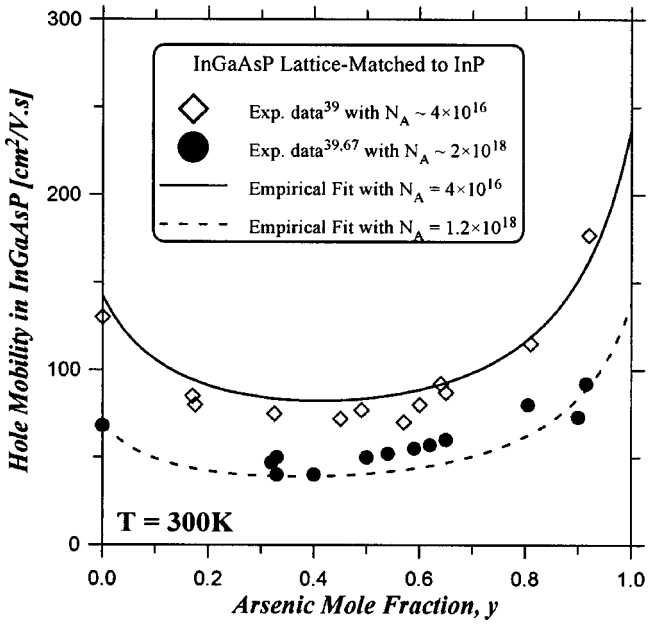

FIG. 12. Hole mobility data (see Refs. 39, 68) of InGaAsP lattice matched to InP vs arsenic mole fraction for the doping concentration 4×10^{16} (open diamonds) and $2\times10^{18}\,\mathrm{cm}^{-3}$ (solid circles) are compared against the empirical curves obtained in this work (lines) for almost similar doping densities.

lation between the mobilities in these two materials results in negative mobility in some range of composition. Therefore, a power interpolation of the following form is adopted:

$$\mu_D(\mathrm{In}_{1-x}\mathrm{Al}_x\mathrm{As}) = (\mu_{n,\max}(\mathrm{InAs},300\,\mathrm{K}))^{(1-x/0.48)} \times (\mu_{n,\max}(\mathrm{In}_{0.52}\mathrm{Al}_{0.48}\mathrm{As},300\,\mathrm{K}))^{(x/0.48)}. \tag{13}$$

A similar formulation is used for $\mu_{n,\min}(\mathrm{In}_{1-x}\mathrm{Al}_x\mathrm{As})$. A quadratic interpolation is used for λ_n and $\mathrm{Log}_{10}(N_{n,\mathrm{ref}},300\,\mathrm{K})$ in this material, while θ_{n2} is linearly interpolated between the corresponding values for InAs and AlAs, and an interpolation scheme similar to Eq. (10) with $m=1$ is used for θ_{n1}.

No reliable data is available in the literature for $\mu_p(\mathrm{In}_{1-x}\mathrm{Al}_x\mathrm{As})$. Therefore, a linear interpolation is used for $\mu_{p,\min}$, $\mathrm{Log}_{10}[N_{p,\mathrm{ref}}(300\,\mathrm{K})]$, λ_p, and θ_{p2}. To take the effect of alloy scattering into account, an interpolation similar to Eq. (10) may be used for $\mu_{p,\max}(300\,\mathrm{K})$ and θ_{p1}.

I. $\mathrm{In}_{1-x}\mathrm{Ga}_x\mathrm{As}_y\mathrm{P}_{1-y}$

Majority of the electron and hole mobility data in the literature for the quaternary material $\mathrm{In}_{1-x}\mathrm{Ga}_x\mathrm{As}_y\mathrm{P}_{1-y}$ belong to the compositions lattice matched to InP (Ref. 6 and references therein; Refs. 39, 67, and 68). Due to the lack of knowledge about the Hall mobilities of $\mathrm{GaAs}_y\mathrm{P}_{1-y}$ and $\mathrm{InAs}_y\mathrm{P}_{1-y}$, only the mobility parameters of $\mathrm{In}_{1-x}\mathrm{Ga}_x\mathrm{P}$ and $\mathrm{In}_{1-x}\mathrm{Ga}_x\mathrm{As}$ are used for interpolation schemes. For instance, λ_n is found using

$$\lambda_n(\mathrm{In}_{1-x}\mathrm{Ga}_x\mathrm{As}_y\mathrm{P}_{1-y}) = y\lambda_n(\mathrm{In}_{1-x}\mathrm{Ga}_x\mathrm{As}) + (1-y)\lambda_n(\mathrm{In}_{1-x}\mathrm{Ga}_x\mathrm{P}). \tag{14}$$

A similar linear interpolation is used for θ_{n2}, $\mathrm{Log}_{10}[N_{n,\mathrm{ref}}(300\,\mathrm{K})]$, λ_p, $\mu_{p,\min}$, θ_{p2}, and $\mathrm{Log}_{10}[N_{p,\mathrm{ref}}(300\,\mathrm{K})]$. $\mu_{n,\max}(300\,\mathrm{K})$ is interpolated using

$$\mu_{n,\max}(\mathrm{In}_{1-x}\mathrm{Ga}_x\mathrm{As}_y\mathrm{P}_{1-y},\ 300\,\mathrm{K}) = \frac{y\mu_{n,\max}(\mathrm{In}_{1-x}\mathrm{Ga}_x\mathrm{As},\ 300\,\mathrm{K}) + (1-y)\mu_{n,\max}(\mathrm{In}_{1-x}\mathrm{Ga}_x\mathrm{P},\ 300\,\mathrm{K})}{1+my(1-y)} \tag{15}$$

with $m=6$. Similarly, Eq. (15) is used for $\mu_{n,\min}(m=6)$, $\theta_{n1}(m=1)$, $\mu_{p,\max}(300\,\mathrm{K})(m=6)$, and $\theta_{p1}(m=1)$. The above values of m are chosen to give a reasonable agreement to the electron and hole mobility data for InGaAsP lattice matched to InP available in the literature (see below). For example, the electron mobility data of InGaAsP lattice matched to InP for the doping range $(1-5)\times10^{16}\,\mathrm{cm}^{-3}$ (Refs. 39, 68) and for relatively pure samples (Ref. 6) are shown in Fig. 11 as a function of arsenic mole fraction, y. Also plotted in this figure is the empirical variation obtained in this work for $N=10^{15}$, 10^{16}, and $5\times10^{16}\,\mathrm{cm}^{-3}$. It is clear from this figure that the empirical formula used in this work predicts the electron mobility data of InGaAsP quite well, and the majority of measured data points are located in the area between the two empirical curves for 10^{15} and $5\times10^{16}\,\mathrm{cm}^{-3}$ doping concentrations. A similar comparison

TABLE II. Values of the static and optical dielectric constants, conduction band effective masses, and direct/indirect band gaps of the III–V binary compounds used in this work. Also the band gap bowing parameters for the ternary compounds are given.

Parameter	Unit	AlAs	GaAs	InAs	InP	GaP
ε_s	ε_0	10.06	12.90	15.15	12.61	11.10
ε_∞	ε_0	8.16	10.92	12.25	9.61	9.08
$E_{g\Gamma}$	eV	2.799	1.422	0.350	1.351	2.760
E_{gX}	eV	2.163	1.899	2.140	2.200	2.261
E_{gL}	eV	2.469	1.707	1.450	2.000	2.630
$m_{n\Gamma}$	m_0	0.150	0.065	0.023	0.079	0.126
m_{nX}	m_0	0.71	0.85	0.64	0.676	0.82
m_{nL}	m_0	0.66	0.56	0.29	0.655	0.756
		Band gap bowing parameters				
	InAlAs	AlGaAs	InGaAs	InGaP	GaAsP	InAsP
b_G (eV)	0.304	0.0	0.42	0.67	0.21	0.286
b_X (eV)	0.713	0.143	0.509	0.17	0.21	0.187
b_L (eV)	0.617	0.15	1.087	0.41	0.42	0.115

has been made in Fig. 12 for the hole mobility data in InGaAsP lattice matched to InP. Again the empirical fits agree quite well with the data points summarized in Refs. 39 and 68. Additionally, using $m=1$ for $\theta_{n1}(\mathrm{In}_{1-x}\mathrm{Ga}_x\mathrm{As}_y\mathrm{P}_{1-y})$ has resulted in a temperature dependence of mobility very similar to those reported[67] for various compositions of InGaAsP lattice matched to InP.

V. CONCLUSIONS

In this work an empirical model for the low-field mobility of III–V compounds as a function of doping concentration, temperature, and composition was developed. Appropriate parameter sets for a large number of binary, ternary, and quaternary compounds were obtained by fitting to a rather numerous available Hall mobility data in the literature. Additionally, suitable interpolation schemes were suggested to determine the electron and hole mobilities of ternary and quaternary III–V alloys in the entire range of composition.

The range of validity of the present mobility model is also discussed. In particular, Eq. (4) with parameter sets given in Table I should not be used for temperatures lower than ~100 K. Modifications to the present model and/or fitting parameters (a temperature dependent λ, for instance) are necessary before one can use this model for very low temperatures. Additionally, the model is suitable for bulk materials and is assumed to be independent of dopant species or the growth method. The results of this work are extremely valuable as input to device simulation packages for improved theoretical prediction of device characteristics.

ACKNOWLEDGMENTS

This work was partly supported by Engineering and Physical Sciences Research Council (EPSRC) of UK. M. Sotoodeh also wishes to acknowledge the financial support of the Ministry of Culture and Higher Education (MCHE) of Iran.

APPENDIX: BAND PARAMETERS AND DIELECTRIC CONSTANTS

The physical parameters of the binary compounds required for the interpolation of mobilities in Eqs. (5), (7), and (12) are summarized in Table II. These data are taken from numerous resources and a detailed discussion of them is given in Ref. 61. For the ternary material $A_xB_{1-x}C$, these parameters are interpolated as follows:[69]

$$E_{gv}(x)=xE_{gv}(AC)+(1-x)E_{gv}(BC) - b(ABC)x(1-x), \tag{A1}$$

$$m_{nv}(x)=xm_{nv}(AC)+(1-x)m_{nv}(BC), \tag{A2}$$

$$\frac{\varepsilon_{s,\infty}(x)-1}{\varepsilon_{s,\infty}(x)+2}=x\frac{\varepsilon_{s,\infty}(AC)-1}{\varepsilon_{s,\infty}(AC)+2}+(1-x)\frac{\varepsilon_{s,\infty}(BC)-1}{\varepsilon_{s,\infty}(BC)+2}. \tag{A3}$$

[1] W. Walukiewicz, J. Lagowski, L. Jastrzebski, M. Lichtensteiger, and H. C. Gatos, J. Appl. Phys. **50**, 899 (1979).
[2] S. Adachi, *GaAs and Related Materials: Bulk Semiconducting and Superlattice Properties* (World Scientific, Singapore, 1994), Chap. 14.
[3] H. S. Bennett, J. Appl. Phys. **80**, 3844 (1996).
[4] S. Adachi, J. Appl. Phys. **58**, R1 (1985).
[5] S. Adachi, J. Appl. Phys. **53**, 8775 (1982).
[6] S. Adachi, *Physical Properties of III–V Semiconductor Compounds: InP, InAs, GaAs, GaP, InGaAs, and InGaAsP* (Wiley, New York, 1992), pp. 223–238.
[7] M. Lundstrom, *Fundamentals of Carrier Transport*, Vol. 10 of *Modular Series on Solid State Devices*, edited by G. W. Neudeck and R. F. Pierret (Addison–Wesley, Reading, MA, 1990), Chap. 2.
[8] D. B. M. Klaassen, Solid-State Electron. **35**, 953 (1992); **35**, 961 (1992).
[9] D. M. Caughey and R. E. Thomas, Proc. IEEE **55**, 2192 (1967).
[10] N. D. Arora, J. R. Hauser, and D. J. Roulston, IEEE Trans. Electron Devices **ED-29**, 292 (1982).
[11] S. Noor Mohammad, A. V. Bemis, R. L. Carter, and R. B. Renbeck, Solid-State Electron. **36**, 1677 (1993).
[12] *MEDICI: Two-Dimensional Semiconductor Device Simulation, User's Manual* (Technology Modeling Associates, Palo Alto, 1993).
[13] *ATLAS User Manual* (Silvaco International, Santa Clara, 1997).
[14] M. L. Lovejoy, M. R. Melloch, and M. S. Lundstrom, Appl. Phys. Lett. **67**, 1101 (1995).
[15] B-C. Lye, P. A. Houston, H-K. Yow, and C. C. Button, IEEE Trans. Electron Devices **45**, 2417 (1998).

[16] M. Wenzel, G. Irmer, J. Monecke, and W. Siegel, Semicond. Sci. Technol. **13**, 505 (1998).
[17] W. Walukiewicz, J. Lagowski, and H. C. Gatos, J. Appl. Phys. **53**, 769 (1982).
[18] W. Walukiewicz, J. Lagowski, L. Jastrzebski, P. Rava, M. Lichtensteiger, C. H. Gatos, and H. C. Gatos, J. Appl. Phys. **51**, 2659 (1980).
[19] D. A. Anderson, N. Apsley, P. Davies, and P. L. Giles, J. Appl. Phys. **58**, 3059 (1985).
[20] *Properties of Gallium Arsenide*, 3rd ed. EMIS Datareviews series No. 16, edited by M. R. Borzel and G. E. Stillman (INSPEC, London, 1996), Chaps. 2, 3, p. 106.
[21] J. R. Meyer and F. J. Bartoli, Phys. Rev. B **36**, 5989 (1987).
[22] P. M. Enquist, Appl. Phys. Lett. **57**, 2348 (1990).
[23] M. C. Hanna, Z. H. Lu, and A. Majerfeld, Appl. Phys. Lett. **58**, 164 (1991).
[24] M. K. Hudait, P. Modak, S. Hardikar, and S. B. Krupanidhi, J. Appl. Phys. **82**, 4931 (1997).
[25] M. Levinshtein, S. Rumyantsev, and M. Shur, *Handbook Series on Semiconductor Parameters*, Vol. 1: *Si, Ge, C (Diamond), GaAs, GaP, GaSb, InAs, InP, InSb* (World Scientific, Singapore, 1996), pp. 84–86, 153–155, 175–177.
[26] S. Selberherr, *Analysis and Simulation of Semiconductor Devices* (Springer, Wien, 1984).
[27] C. Algora and V. Diaz, Solid-State Electron. **41**, 1787 (1997).
[28] S. Selberherr, W. Hansch, M. Seavey, and J. Slotboom, Solid State Electron **33**, 1425 (1990).
[29] J. E. Sutherland and J. R. Hauser, IEEE Trans. Electron Devices **ED-24**, 363 (1977).
[30] S. Adachi (editor), *Properties of Aluminium Gallium Arsenide*, EMIS Datareviews Series No. 7, edited by S. Adachi (INSPEC, London, 1993), pp. 167–170.
[31] S. Fujita, S. M. Bedair, M. A. Littlejohn, and J. R. Hauser, J. Appl. Phys. **51**, 5438 (1980).
[32] H. Kressel and J. K. Butler, *Semiconductor Lasers and Heterojunction LEDs* (Academic, New York, 1977), pp. 332, 333, 348–353.
[33] *Properties of Indium Phosphide*, EMIS Datareviews Series No. 6, edited by S. Adachi (INSPEC, London, 1991), Chaps. 4, 5, p. 400.
[34] M. Razeghi, *The MOCVD Challenge, Vol. 1: A Survey of GaInAsP-InP for Photonic and Electronic Applications* (Hilger, London, 1989).
[35] G. H. Olsen and T. J. Zamerowski, IEEE J. Quantum Electron. **QE-17**, 128 (1981).
[36] S. F. Yoon, H. Q. Zheng, P. H. Zhang, K. W. Mah, and G. I. Ng, Jpn. J. Appl. Phys., Part 1 **38**, 981 (1999).
[37] S. Tiwari, *Compound Semiconductor Device Physics* (Academic, New York, 1992).
[38] P. A. Postigo, M. L. Dotor, P. Huertas, F. Garcia, D. Golmayo, and F. Briones, J. Appl. Phys. **85**, 6567 (1999).
[39] G. P. Agrawal and N. K. Dutta, *Semiconductor Lasers*, 2nd ed. (Van Nostrand Reinhold, New York, 1993), pp. 170–172.
[40] Y. C. Kao and O. Eknoyan, J. Appl. Phys. **54**, 2468 (1983).
[41] Y. Ohba, M. Ishikawa, H. Sugawara, M. Yamamoto, and T. Nakanishi, J. Cryst. Growth **77**, 374 (1986).
[42] Epitaxial Products International, Cardiff, UK (private communication).
[43] J. H. Quigley, M. J. Hafich, H. Y. Lee, R. E. Stave, and G. Y. Robinson, J. Vac. Sci. Technol. B **7**, 358 (1989).
[44] S. P. Najda, A. Kean, and G. Duggan, J. Appl. Phys. **82**, 4408 (1997).
[45] III–V Semiconductor Centre, University of Sheffield, UK (private communication).
[46] P. Blood, J. S. Roberts, and J. P. Stagg, J. Appl. Phys. **53**, 3145 (1982).
[47] C. C. Hsu, J. S. Yuan, R. M. Cohen, and G. B. Stringfellow, J. Appl. Phys. **59**, 395 (1986).
[48] M. Razeghi, *The MOCVD Challenge, Vol. 2: A Survey of GaInAsP-GaAs for Photonic and Electronic Device Applications* (IOP, Bristol, 1995).
[49] T. Shitara and K. Eberl, Appl. Phys. Lett. **65**, 356 (1994).
[50] M. Ikeda and K. Kaneko, J. Appl. Phys. **66**, 5285 (1989).
[51] B. R. Nag and M. Das, J. Appl. Phys. **83**, 5862 (1998).
[52] Y. Hsu, G. B. Stringfellow, C. E. Inglefield, M. C. DeLong, P. C. Taylor, J. H. Cho, and T-Y. Seong, Appl. Phys. Lett. **73**, 3905 (1998).
[53] W. T. Masselink, M. Zachau, T. W. Hickmott, and K. Hendrickson, J. Vac. Sci. Technol. B **10**, 966 (1992).
[54] J. B. Lee, S. D. Kwon, I. Kim, Y. H. Cho, and B-D. Choe, J. Appl. Phys. **71**, 5016 (1992).
[55] J. M. Kuo and E. A. Fitzgerald, J. Vac. Sci. Technol. B **10**, 959 (1992).
[56] D. Biswas, H. Lee, A. Salvador, M. V. Klein, and H. Morkoc, J. Vac. Sci. Technol. B **10**, 962 (1992).
[57] S. F. Yoon, K. W. Mah, and H. Q. Zheng, J. Appl. Phys. **85**, 7374 (1999).
[58] H. Sai, H. Fujikura, and H. Hasegawa, Jpn. J. Appl. Phys., Part 1 **38**, 824 (1999).
[59] S. Courmont, Ph. Maurel, C. Grattepain, and J. Ch. Garcia, Appl. Phys. Lett. **64**, 1371 (1994).
[60] L. B. Chang, K. Y. Cheng, and C. C. Liu, J. Appl. Phys. **64**, 1116 (1988).
[61] M. Sotoodeh, Ph.D. Dissertation, King's College London, to be submitted, April 2000.
[62] F. Fuchs, K. Khang, P. Koidl, and K. Schwarz, Phys. Rev. B **48**, 7884 (1993).
[63] *Properties of Lattice-Matched and Strained Indium Gallium Arsenide*, EMIS Datareviews Series No. 8, edited by P. Bhattacharya (INSPEC, London, 1993), pp. 103–105, 112.
[64] P. W. Yu and E. Kuphal, Solid State Commun. **49**, 907 (1984).
[65] T. Fujii, T. Inata, K. Ishii, and S. Hiyamizu, Electron. Lett. **22**, 191 (1986).
[66] S. Goto, T. Ueda, T. Ohshima, and H. Kakinuma, Jpn. J. Appl. Phys., Part 1 **38B**, 1048 (1999).
[67] P. K. Bhattacharya, J. W. Ku, S. J. T. Owen, G. H. Olsen, and S-H. Chiao, IEEE J. Quantum Electron. **QE-17**, 150 (1981).
[68] K. Tappura, J. Appl. Phys. **74**, 4565 (1993).
[69] S. Adachi, *Physical Properties of III-V Semiconductor Compounds: InP, InAs, GaAs, GaP, InGaAs, and InGaAsP* (Wiley, New York, 1992), Appendix.